Electrochemical Formation and Reactivity of a Mn-Peroxo Complex Bearing an Amido N5 Ligand

Allyssa Massie, Nikolaos Kostopoulos, Elizabeth Grotemeyer, Jean-marc Noël, Timothy Jackson, Elodie Anxolabéhère-Mallart

Electrochemical formation and reactivity of a Mn peroxo complex bearing an amido N5 ligand

Allyssa A. Massie, [a] Nikolaos Kostopoulos, [b] Elizabeth N. Grotemeyer,[a] Jean-Marc Noël,[c] Timothy A. Jackson,*[a] Elodie Anxolabéhère-Mallart*[b]

Dedicated to Professor Jean-Michel Savéant

[a] Dr. A.A. Massie, E.N. Grotemeyer, Dr. T.A.Jackson
Department of Chemistry
University of Kansas
1567 Irving Hill Road, Lawrence, KS 66045
E-mail: taj@ku.edu

[b] Dr. N. Kostopoulos, Dr. E. Anxolabéhère-Mallart
Laboratoire d'Electrochimie Moléculaire
Université Paris Cité, CNRS
15, rue Jean-Antoine de Baïf, Paris Cedex 13
E-mail: elodie.anxolabehere@u-paris.fr

[c] Dr J.-M. Noël
ITODYS
Université Paris Cité, CNRS
15, rue Jean-Antoine de Baïf, Paris Cedex 13

Supporting information for this article is given via a link at the end of the document.

Abstract: Herein we report the electrochemical generation of a mononuclear Mn^{III}(OO) (peroxo) complex supported on a dpaq ligand (dpaq = 2-(bis(pyridin-2-ylmethyl)amino)-N-(quinolin-8-yl)acetamide) for the first time, and its reactivity in *N,N*-dimethylformamide. The formation of the Mn^{III}(dpaq)(OO) complex is probed by low temperature electronic absorption spectro-electrochemistry experiments. An analysis of the reduction of the Mn^{III}(dpaq)(OO) complex is carried out combining cyclic voltammetry and simulations. The involvement of a Mn^{II}(dpaq)(OOH) complex is proposed based on CV data, and is corroborated by DFT computations.

Introduction

Manganese ions are found in the active sites of several enzymes, such as Mn superoxide dismutase (MnSOD) that catalyzes the transformation of superoxide ion ($O_2^{\bullet-}$) to O_2 and H_2O_2,[1] the Mn catalase that transforms H_2O_2 to H_2O,[2] and the Mn lipoxygenase that introduces -OOH groups to fatty acids.[3] A Mn cluster is also present in the oxygen evolving center (OEC) of photosystem II.[4] This multi-manganese cluster is responsible for splitting water into O_2, protons, and electrons (the oxygen-evolution reaction, or OER). Scheme 1 summarizes some of these enzymatic transformations.

$$2O_2^{\bullet-} + 2H^+ \longrightarrow H_2O_2 + O_2 \quad Mn\text{-}SOD$$

$$2H_2O_2 \longrightarrow O_2 + 2H_2O \quad Mn\text{-}catalase$$

$$2H_2O \longrightarrow 4H^+ + 4e^- + O_2 \quad Photosystem\ II$$

Scheme 2 : Reactions catalyzed by Mn containing enzymes

Mn^{III}(OO) (peroxo) and Mn^{II}(OOH) (hydroperoxo) species have been described as key intermediates in the OER of the OEC,[5] and in the MnSOD enzyme. Peroxo and hydroperoxo adducts of other metals, such as Fe and Cu, play key roles in the oxygen reduction reaction (ORR) and in aerobic oxidation of substrates by heme, nonheme, and Cu-dependent enzymes.[6]

In the case of manganese, several mononuclear Mn-peroxo complexes have been reported in the literature. Typically, non-porphyrinic Mn-peroxo complexes are generated from the reaction of Mn^{II} or Mn^{III} precursors with KO_2 (potassium superoxide)[7] or H_2O_2.[8] More rarely, these adducts are formed using O_2 in the presence of reducing equivalents[9] and using pulsed radiolysis.[10] Mn-peroxo complexes supported by porphyrin ligands have also been described.[11] In the studies where structural information was obtained, the peroxo is bound in a side-on mode.[8a, 8h] In cases lacking experimental structure determination, DFT calculations predict six coordinate structures, with the ancillary ligand bound in a tetradentate manner.[8d, 8f]

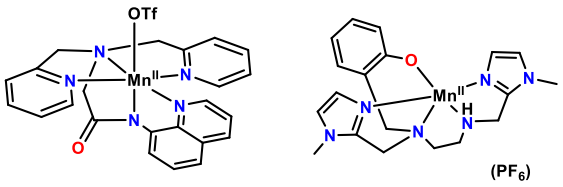

Scheme 1 : Left: Structure of the Mn complex under study. Right: Structure of the Mn complex studied in ref 16.

As an alternative approach to the production of metal-peroxo adducts by chemical means, we have employed electrochemical methods to prepare and spectroscopically characterize Mn-peroxo and Fe-peroxo complexes featuring both non-porphyrinic[12],[13] and porphyrin[14],[15] supporting ligands. In the studies describing non-heme Mn peroxo complexes,[12, 16] the Mn^{II} complex is dissolved in O_2-saturated solution in an electrochemical cell and a potential is applied such that O_2 is reduced to $O_2^{\bullet-}$ at the electrode surface. This electrochemically-generated $O_2^{\bullet-}$ reacts with the reduced metal center to yield the corresponding metal(III)-peroxo adduct. Specifically, with a series of Mn complexes supported by non-porphyrinic pentadentate ligand L, we have demonstrated that the Mn^{III}(L)(OO) adducts can be prepared by reaction of the starting Mn^{II} complex with *in situ* electrochemically generated $O_2^{\bullet-}$.[12] In this case, the yields of the Mn^{III}(L)(OO) adducts formed by this electrochemical process were higher than those achieved by chemical oxidation. Further-more, we showed that a Mn^{III}(L)(OO) supported on a phenolato-containing ligand reacts with strong Brønsted-Lowry acids to cleave the Mn-O bond and produce H_2O_2. In contrast, O-O cleavage of the Mn^{III}(L)(OO) complex occurs with its reduction in the presence of water.[16]

Herein we have electrochemically prepared for the first time a Mn^{III}(dpaq)(OO) complex supported in the non-porphyrinic pentadentate ligand (dpaq) featuring an amide moiety (scheme 2). The initial Mn^{II}(dpaq)(OTf) complex has been previously shown to activate O_2 by some of us under non-electrochemical conditions.[17] However, the reactivity of this complex with O_2 in DMF and $O_2^{\bullet-}$ has been unexplored. In the present paper, we study the electro-chemical O_2 activation by Mn^{II}(dpaq)(OTf), using cyclic voltammetry, UV-Vis spectroelectrochemistry, CV simulations and DFT computations. This work highlights the role of the supporting ligand on the reactivity of Mn^{III}(OO) unit upon electron transfer.

Results and Discussion

Figure 1A shows the cyclic voltammograms (CV) obtained in Ar saturated DMF solution of Mn^{II}(dpaq)(OTf) complex. DMF is a convenient solvent to study O_2 activation because Mn^{II}(dpaq)(OTf) does not react with O_2 spontaneously in DMF, in contrast to acetonitrile.[18] This behavior can be attributed to the nature of the solvent coordination in the metal center, which is stronger in the case of DMF, and prevents the introduction of the O_2 in the coordination sphere of the Mn(II).[17d] Two oxidation features (p_1 and $p_{1'}$) and one reduction feature ($p_{1''}$) are present. The p_1 at $E^p \approx 0.7$ V is attributed to the one electron irreversible oxidation of Mn^{II}(dpaq)(OTf) into the corresponding Mn^{III} complex. The irreversibility of Mn^{II}/Mn^{III} redox process is known to originate from changes of the coordination sphere of the Mn(II) center upon oxidation.[19] The $p_{1'}$ and $p_{1''}$ features are, on the other hand, attributed to ligand centered oxidation and reduction, respectively, based on the CV of the dpaq ligand in the same conditions (See Figure S1).

In air saturated DMF solutions, a new reduction peak is present with a $E^p \approx -0.8$ V (p_2) that is followed by a re-oxidation peak at $E^p \approx 0.4$ V, (p_3) (Figure 1B). Based on our previously reported studies[16] for other Mn^{II} non-porphyrinic complexes we propose that $p_2$corresponds to the reduction of O_2 to $O_2^{\bullet-}$ followed by the reaction between $Mn^{II}(dpaq)^+$ and $O_2^{\bullet-}$ to give the Mn^{III}(dpaq)(OO) complex according to the EC mechanism shown in Scheme 3, (see SI Figure S2, for CV simulation). Noteworthy, on the reverse scan (reoxidation of $O_2^{\bullet-}$ to O_2, a discrepancy between the

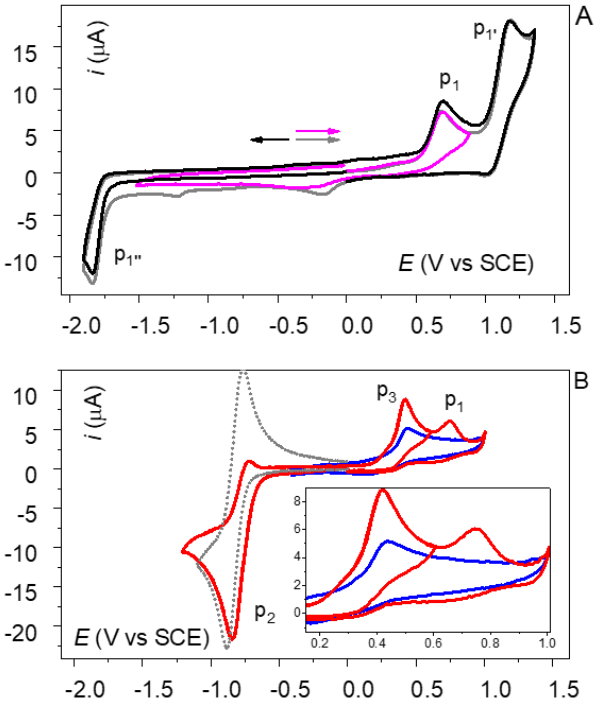

Figure 1 A: CV of 1.1 mM of Mn^{II}(dpaq)(OTf) in argon saturated DMF with 0.1 M $TBAPF_6$ on glassy carbon electrode with d=0.3 cm at v= 0.1 V/s, T = 293 K, in different potential windows. B: Air saturated solution (red traces, different potential windows) and argon saturated solution after addition of 1.2 eq of KO_2 (blue trace) at 253 K. The $O_2/O_2^{\bullet-}$ is shown as grey dotted trace for comparison. Inset: zoom of the p_1 and p_3 oxidation peaks

simulation and the experiment even at different scan rate (Figure S3) could be observed according to what was reported previously.[16] As shown in Figure S4, this can be attributed to undesired surface phenomena. More importantly, towards more anodic potential, the p_3 corresponds to the reoxidation of the latter to a formal $[Mn^{IV}(dpaq)(OO)]^+$ complex, possibly releasing Mn^{II} and O_2, as we have previously reported.[12, 16]

Reaction of Mn^{II} with KO_2 can also lead to the formation of the Mn^{III}(OO) complex . In the case of Mn^{II}(dpaq)(OTf), addition of a small excess of KO_2 in Ar saturated DMF leads to the appearance of a peak (Figure 1B, blue trace) with the same potential as p_3, supporting our attribution of this peak to the oxidation of Mn^{III}(dpqa)(OO).

$$E \qquad O_2 + e^- \rightleftharpoons O_2^{\bullet-}$$

$$C \qquad [Mn^{II}(dpaq)]^+ + O_2^{\bullet-} \underset{}{\overset{K_{O_2^{\bullet-}}}{\rightleftharpoons}} [Mn^{III}(dpaq)(OO)]$$

Scheme 3. Reaction of Mn^{II} complex with superoxide

Thin layer electronic absorption spectroelectrochemistry experiments provide further evidence for the formation of the Mn^{III}(OO) complex. Figure 2 shows the evolution of the UV-Vis spectrum of an air saturated DMF solution of Mn^{II}(dpaq)(OTf) recorded in a spectroelectrochemical cell upon applying a potential of -1.1 V vs SCE. After 10 min, two new absorption features appear: a low intensity broad band at ~ 600 nm and a

sharper and more intense peak at 430 nm. The spectrum of a solution resulting from addition of KO_2 to argon saturated solution of Mn^{II}(dpaq)(OTf) displays similar features at 600 nm and 430 nm, thus supporting the attribution of these new features to those characteristic of the Mn^{III}(dpaq)(OO) peroxo complex (see Figure S5).

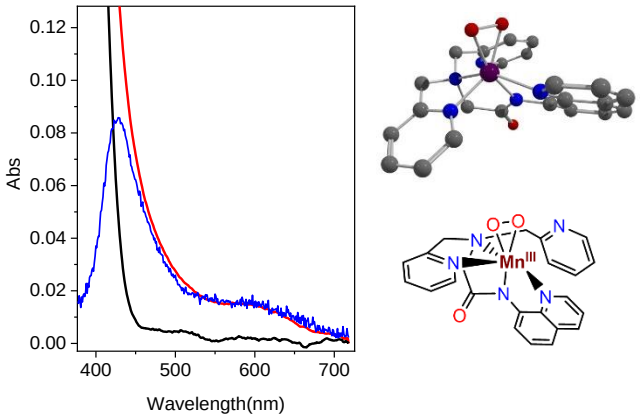

Figure 2 : Left: UV-Vis spectroelectrochemistry of 1.1 mM of Mn^{II}(dpaq)(OTf) in air saturated ([O_2] = 1 mM) DMF solution with 0.2 M $TBAPF_6$. WE: Carbon paper. Electrolysis at -1.1 V vs SCE. Optical path 0.1 cm, at 253 K. Black trace: Mn^{II}, before electrolysis, red trace: peroxo, after 10 min electrolysis. Blue trace: linear subtraction (non-smoothed). Right: The DFT optimized structure for [$Mn^{III}(O_2)$(dpaq-py)] is shown on the right. Geometry optimizations were performed with the TPSS functional and the def2-TZVP (Mn, O, and N atoms) and def2-SVP (C and H atoms) basis sets.

DFT computations also provide support that the species observed by spectroelectrochemistry corresponds to the Mn^{III}(dpaq)(OO) complex. Three different structures of Mn^{III}(dpaq)(OO) were considered: one in which the dpaq ligand remains bound in a pentadentate fashion and structures in which either the quinoline or one of the pyridine arms are dissociated (Figure S10). Each of these structures features a side-on peroxo ligand with a short O-O bond (1.42 – 1.45 Å, Table S2), consistent with a Mn^{III}-peroxo species. The lowest energy structure is the 6-coordinate structure in which the pyridine is dissociated (Figure 2); however, the 7-coordinate structure is only ~4 kcal mol^{-1} higher in energy, suggesting that such a structure is still feasible and precluding definitive identification of the experimental species on the basis of the optimized geometries alone (Table S2).

TD-DFT calculations were performed for each Mn^{III}(dpaq)(OO) species in order to determine which structures best reproduce the experimental absorption spectrum (Figure 2); TD-DFT calculations used the B3LYP functional and the same basis sets as used for geometry optimizations). The TD-DFT absorption spectra for Mn^{III}(dpaq-py)(OO) and Mn^{III}(dpaq-qn)(OO), where -py (pyridine) and -qn (quinolone) indicators show the moiety that is decoordinated, are in good agreement with the experimental data (Figures 2 and S10). Each of these structures has a feature at 610 nm that arises from a Mn^{III} d-d transition from a d_z^2–based orbital to a d_{xy}-based MO (see Supporting Information). In these calculations, the z-axis is perpendicular to the plane of the Mn^{III}-peroxo unit, which gives the d_z^2-based MO σ-antibonding interactions with many of the dpaq donors, while the d_{xy} MO shows a strong σ-antinbonding interaction between the Mn^{III} center and the in-plane π* MOs of the peroxo unit (see Tables S3-5). For the seven-coordinate Mn^{III}(dpaq)(OO) species, the computed absorption spectrum is quite different from both the experimental spectrum and the calculated spectra for Mn^{III}(dpaq-py)(OO) and Mn^{III}(dpaq-qn)(OO) with prominent features at 760 nm and 550 nm. These bands arise from Mn $d_z^2 \longrightarrow d_{yz}$ and Mn $d_{x^2-y^2} \longrightarrow d_{yz}$ transitions, respectively (Figure S11, Table S5). The differences in the calculated electronic absorption spectra support the assignment of the experimentally observed Mn^{III}(OO) species as Mn^{III}(dpaq-py)(OO) as this complex is lowest in energy and best reproduces the experimental electronic absorption spectrum.

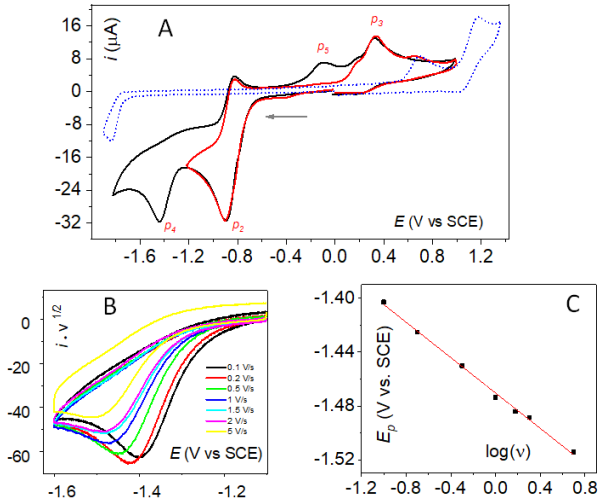

Figure 3 : A: CV of 1.1 mM of Mn^{II}(dpaq)(OTf) in DMF with 0.1 M $TBAPF_6$ on glassy carbon electrode with d=0.3 cm at v= 0.1 V/s, T = 293 K. Argon saturated (blue dotted trace), air saturated (black and red traces, different potential window). B: CVs of the air saturated solution at different scan rates after a 20 second pre-electrolysis at -1.1 V vs SCE. 0.1 V/s (black trace), 0.2 V/s (red trace), 0.5 V/s (light green trace), 1 V/s (blue trace), 1.5 V/s (cyan trace), 2 V/s (violet trace), 5 V/s (yellow trace). C: Variation of the peak potential of p2 with respect to the scan rate: $\partial E/\partial \log v$=-59 mV.

The reactivity of the electrochemically generated Mn^{III}(OO) complex has been evaluated in DMF solutions using cyclic voltammetry and simulations with DigiElch software. As shown in Figure 3, in air saturated solutions of the Mn^{II}(dpaq)(OTf) complex a second irreversible reduction peak, called p_4, appears at $E^p \approx -1.45$ V. The variation of the peak potential with scan rate gives a $\partial E/\partial \log v$=-59 mV that is characteristic of a fast electron transfer step. The transfer coefficient has also been evaluated using the peak width, and the obtained value is also in accordance with a fast electron transfer (see SI section for further details).[20] These observations support a simple EC mechanism where the electron transfer is non-dissociative. [21] A plausible explanation of this feature is a reduction of the Mn^{III}(OO) adduct to Mn^{II}(OO) that, due to its high basic character, is immediately protonated by residual water to give a Mn^{II}(OOH). The intensity of the p_4 feature suggests a one electron process, as confirmed by simulations (see Figure S7).

On the reverse scan towards anodic potentials, a new peak is observed at ~ - 0.1 V (peak p_5 see Figure 3). Based on the simple EC mechanism that we propose, this anodic peak could correspond to the oxidation of the Mn^{II}(OOH) species. To gain further insight on these features we performed CV experiments with varying water concentration of the DMF solutions.

As shown in Figure 4, by adding H_2O into the air saturated DMF solutions of Mn^{II}(dpaq)(OTf) we make the following observations. The p_4 does not evolve, showing that the possible protonation

reaction after the one electron reduction is not rate determining, and excluding a catalytic pathway that would lead to increase of the current. At the same time, the p_5 increases with a concomitant decrease of the p_3. Further investigation of this concomitant process was performed by plotting the current of p_5 and p_3 (i_5 and i_3 respectively) and the sum $i_5 + i_3$ with the concentration of H_2O. A linear relationship with contrary slopes is found for i_5 and i_3 versus log [H_2O] whereas $i_3 + i_5$ remains constant. Interestingly, as detailed in Figure S8, based on this linear relationship one can estimate the residual amount of [H_2O] ~ 30 ± 10mM in DMF (black CV in Figure 4A), a value within the range of those already

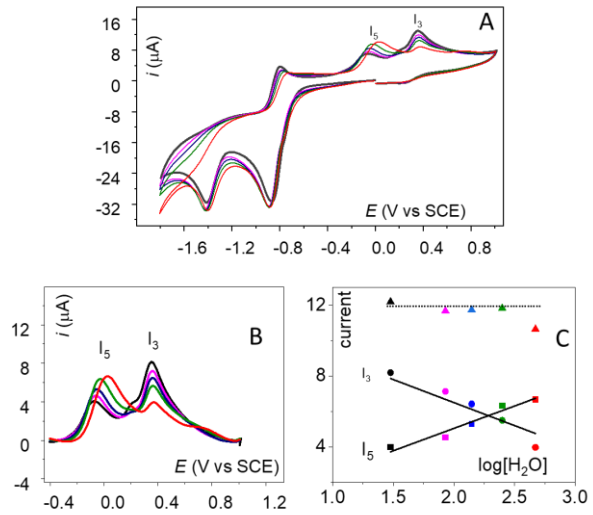

Figure 4 A: CV of 1.1 mM of Mn^{II}(dpaq)(OTf) in DMF with 0.1 M TBAPF6 on glassy carbon electrode with d=0.3 cm at v= 0.1 V/s, T = 293 K. Air saturated solution without added H_2O (black line), with 55 mM (pink line), 110 mM (light blue), 220 mM (blue), 440 mM (red trace). B: Zoom of A on the reoxidation peaks C: Variation of the peak current of p3, p5, and of their addition, with log[H_2O]. We roughly consider the residual H_2O equal to 30 mM (see SI section).

reported.[22] The contrary slopes obtained shows a direct correlation between the decrease of i_3 and the increase of i_5. Moreover, the constant value of $i_5 + i_3$ reflects a conservation of the current of these two oxidation processes when adding H_2O in solution. Given that p_3 corresponds to the oxidation of the Mn^{III}(OO) species and assuming that both oxidations are monoelectronic, our observations suggests that p_5 corresponds to the oxidation of a new mononuclear Mn species, that shares redox and acid-base counterparts. Based on these arguments we propose a reaction scheme where the Mn^{III}(OO) adduct is reduced to a Mn^{II}(OO) that is protonated by water to give a Mn^{II}(OOH) species; the latter is oxidized at p_5. Higher concentrations of water favor the formation of Mn^{II}(OOH) at the expense of Mn^{III}(OO).

To the best of our knowledge, a formal Mn^{II}(OOH) structure with a non-porphyrinic ligand has never been reported before. However there are two examples of $Mn^{II}O_2R$ type species, one from an enzyme[23] and one from a model system prepared by Moro-oka.[24]The proposed reaction scheme (see Scheme 4) was then assessed from simulations of the experimental CV. The values for the various constants are shown in the Table S1. Overall, a satisfactory fit between simulations and experiments is achieved as shown in Figure 5. Variation of Mn complex concentration or content of water are shown in Figure S9. Remarkably, using our simple reaction scheme, the simulated CV (Figure S9) quantitatively reproduce the experimental CV evolution upon addition of water (Figure 4), where adding water results in an increase of p_5 at the expense of the p_3 corroborating our attribution of the newly generated mononuclear species to a Mn^{II}(OOH). A point of discrepancy between the experiment and the simulation is the reoxidation peak of $O_2^{\cdot-}$ to O_2. A plausible rationale for this observation is the various surface phenomena which can have an important impact on the experimental CV but cannot be taken into consideration for the simulations.

As a complement to these simulations, we used DFT calculations to predict reduction potentials for the Mn^{III}(OO)/Mn^{II}(OO), Mn^{III}(OO)/Mn^{IV}(OO), and Mn^{III}(OOH)/Mn^{II}(OOH) couples considered in the simulation (Table S6). Remarkably, the potentials obtained for the Mn^{III}(dpaq-py)(OO) structure, which was favored on the basis of its energy and TD-DFT absorption spectrum, were in good agreement with those obtained from simulations of the experimental CV data. For example, the DFT computations predict potentials of -1.46 V and -0.12 V for the Mn^{III}(OO)/Mn^{II}(OO) and Mn^{II}(OOH)/ Mn^{III}(OOH) couples, respectively, which are very similar to the simulated and experimental values of -1.4 V and -0.10 V (Table S1).[25]

The DFT calculations predict a potential for the Mn^{III}(OO)/Mn^{IV}(OO) couple of 0.58 V (Table S6), which is higher than the experimental value of 0.35 V. In this case, the lack of good agreement likely stems from the paucity of reference potentials for similar complexes with which to benchmark the calculations. For completeness, we calculated potentials for the additional models of Mn^{III}(dpaq)(OO) (Table S6). While these two other structures provided fair agreement with the experimental values for the Mn^{III}(OO)/Mn^{IV}(OO) potential, the calculated

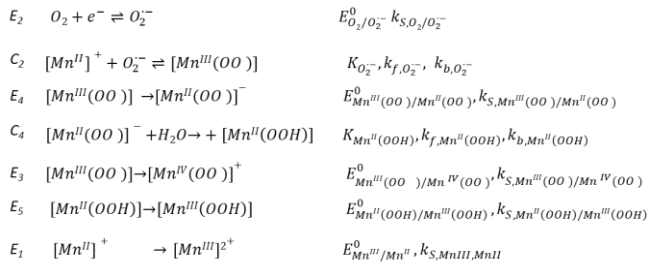

Scheme 4: Equation of the chemical and electrochemical reactions taken into consideration. For the values of the constants see Table S1. Diffusion coefficient for all the Mn species diffusion coefficient D_{Mn} was $4*10^{-6}$ cm^2s^{-1}, for O_2 $4.5*10^{-5}$ cm^2s^{-1} and for superoxide $1.2*10^{-5}$ cm^2s^{-1}. The value of α was taken as 0.5 for all the electron transfers. Initial H_2O was considered to be 30 mM.

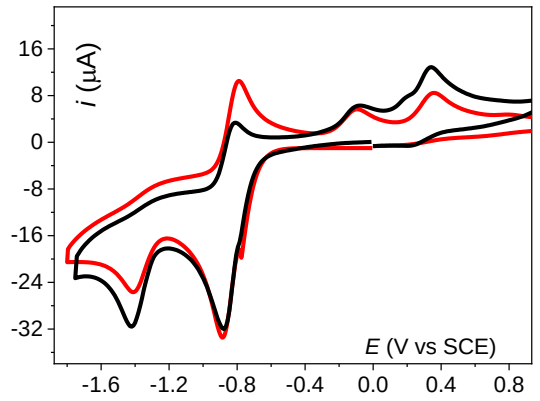

Figure 5: CV of 1.1 mM of Mn^{II}(dpaq)(OTf) in air saturated DMF with 0.1 M $TBAPF_6$ on glassy carbon electrode with d=0.3 cm, at v= 0.1 $V.s^{-1}$, T = 293 K (black trace). Simulation (red trace) taking into considerations the reactions described in scheme 3 with [H_2O] = 30 mM.

potentials for Mn^{II}(OOH)/ Mn^{III}(OOH) couple gave an error of over 0.5 V (-0.63 to -0.64 V).

Discussion:

In this work, we have used a combination of experimental and computational methods to study the formation and reactivity of a new Mn^{III}-peroxo complex and probe its electrochemical properties. Good agreement between experiment and theory supports the set of reactions in Scheme 4, which highlight the importance of both redox and protonation reactions. The very good agreement in the calculated reduction potential of Mn^{III}(dpaq)(OOH) to give a Mn^{II}(dpaq)(OOH) species is particularly intriguing. In previous studies using Mn^{III}(L)(OO) (LH = *N*-(2-hydroxybenzyl)-*N*,*N*-bis[2-(*N*-methylimidazolylmethyl] ethane-1,2-diamine), reduction of Mn^{III}(L)(OO) in the presence of a weak acid resulted in O-O bond cleavage, generating the bis-oxomanganese(IV) species $[Mn^{IV}(L)(O)_2]^-$ rather than the hydroperoxo species.[16] To understand the differences in mechanism upon reduction of the Mn^{III}(dpaq)(OO) and Mn^{III}(L)(OO) complexes, we compared the electronic structures of the hypothetical Mn^{II}-peroxo adducts for the dpaq and L ligands (Figure S13 and S14 respectively). Analysis of the spin density plot of the $[Mn^{II}(dpaq)(OO)]^-$ complex reveals large, positive spin density at *both* the Mn center (4.02) and the quinoline moiety (0.83), and positive and negative spin density on the peroxo ligand (Figure 6). For comparison, the spin density of the Mn^{III}(dpaq)(OO) complex shows positive spin density on the Mn (4.01) and positive and negative spin density on the peroxo, with no spin density on the quinoline group (0.05) (Figure S13). Thus, the change in spin density for the Mn^{III}(dpaq)(OO) and $[Mn^{II}(dpaq)(OO)]^-$ complexes indicates that the reduction does not occur at the manganese center (Figures 6 and S13). Instead, the positive spin density on the quinoline moiety of the $[Mn^{II}(dpaq)(OO)]^-$ complex suggests that a ligand reduction has occurred. (Figures 6 and S13). In further support of this proposal, we observe essentially identical O-O bond lengths for the $[Mn^{II}(dpaq)(OO)]^-$ and Mn^{III}(dpaq)(OO) complexes (1.46 and 1.45 Å, respectively; see Table S2). Thus, the unstable intermediate occurring from the one electron reduction of the Mn^{III}(dpaq)(OO) is better formulated as $[Mn^{III}(dpaq^{-})(OO)]^-$. Redox activity of the dpaq ligand has been proposed previously in the reaction of $[Cu^{II}(dpaq)]^+$ with O_2 resulting in the formation of a Cu^{II}-OOH intermediate and the release of H_2O_2.[26] In that case, the 1-electron reduced species also had significant spin density on the quinoline ligand. Ligand involvement has also been proposed for an oxygen evolution reaction using $[Co^{III}(dpaq)(Cl)]^+$.[27]

The ligand-centered reduction of Mn^{III}(dpaq)(OO) differs remarkably from that proposed for reduction of the $Mn^{III}(L)(O_2)$ complex. In that case, the one-electron reduced $[Mn^{III}(L)(O_2)]^-$ complex shows positive spin density on only the Mn and peroxo centers (Figure 6, right). In addition, the O-O bond in the Mn^{III}(L)(OO) complex is significantly elongated (from 1.46 Å in the Mn^{III}(OO) species to 1.54 Å in the Mn^{II}(OO) species). We propose that this reduction event, which is localized on the Mn-peroxo unit, thus primes the molecule for O-O cleavage[16, 28]

Conclusion

In conclusion, a mononuclear Mn^{III}(OO) (peroxo) complex has been generated from the reaction of electrochemically-generated superoxide with the $[Mn^{II}(dpaq)](OTf)$ complex (dpaq = pentadentate, amide-containing ligand). The Mn^{III}(OO) complex is characterized by UV-Vis spectroelectrochemistry experiments (λ_{max} = 600 and 430 nm) performed in DMF at low temperature. Similar spectral features are observed for an intermediate generated by the chemical reaction of Mn^{II}(dpaq)(OTf) with KO_2. An analysis of the reduction of the Mn^{III}(OO) complex by cyclic voltammetry combined with simulations reveals an EC process consisting of a fast electron transfer and subsequent protonation to yield a Mn^{II}(OOH) (hydroperoxo) product. Thus, reduction of the Mn^{III}(OO) unit leaves the O-O bond intact. This result contrasts with prior studies of a Mn^{III}(OO) adduct coordinated by a phenolate-containing ligand. DFT computations suggest that the differences in the reduction behavior of these complexes stems from redox activity for the amide-containing dpaq ligand.

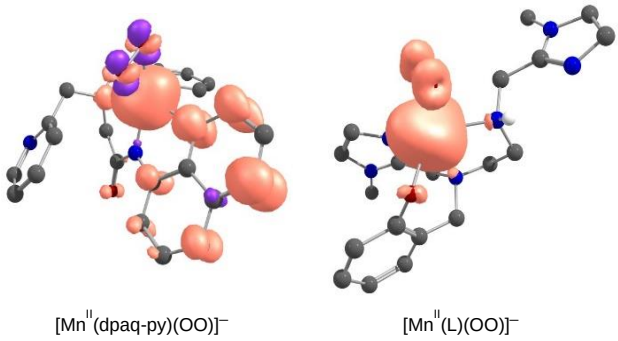

Figure 6. Spin density plots of $[Mn^{II}(dpaq\text{-}py)(OO)]$ (left) and $[Mn^{II}(L)(OO)]$ (right) with one of the methylimidazole arms dissociated.

Experimental Section

The free ligand, Hdpaq, and metal complex $[Mn^{II}(dpaq)](OTf)$ were made as previously described.[29] Details for all electronic structure computations are included in the Supporting Information.

Chemicals.

All reagents and solvents were obtained commercially (Sigma-Aldrich). Tetrabutylammonium hexafluorophosphate ($TBAPF_6$) supporting electrolyte, N,N-dimethylformamide (DMF, anhydrous, 99.8%, ACROS), were used without further purification.

Cyclic Voltammetry.

Electrochemical experiments were run under an argon or O_2 atmosphere. A dry O_2 atmosphere was obtained by purging the solution with compressed air via a glass tube filled with $CaCl_2$. Cyclic voltammograms were recorded on a Metrohm potentiostat (AUTOLAB Model PGSTAT302N). For cyclic voltammetry, the counter electrode used was a Pt wire and the working electrode a glassy-carbon disk (3 mm diameter) carefully polished before each voltammogram with a 1 µm diamond paste, sonicated in an ethanol bath, and then washed with ethanol. The reference electrode used was an SCE (saturated calomel electrode), isolated from the rest of the solution with a fritted bridge. The supporting electrolyte had a concentration of 0.1 M (293 K) or 0.2

M (253 K). Low-temperature regulation was ensured by a Julabo circulation cryostat.

UV−Visible Spectroelectrochemistry.
Thin-cell spectroelectrochemical data were obtained using a combination of three electrodes in a thin cell (optical length 0.2 cm) mounted on a UV/vis Varian Cary 60 spectrophotometer, equipped with a transparent Dewar.34 It consists of a 0.1 cm quartz UV−vis− NIR cell surmounted by a glass compartment. A homemade carbon (Alfa Aesar) electrode was used as the working electrode, a carbon/Teflon in a frit as the reference electrode, and a platinum grid in a frit as the counter electrode. The entire solution was saturated with air (1 mM O_2), and the cell was cooled to 253 K by a Julabo circulation cryostat. Spectroelectrochemistry was also performed in a larger cuvette of 1 cm, using a similar set-up.

Electronic Structure Calculations. Density functional theory calculations were performed for all species using the ORCA 4.2 software program.[30] Geometry optimizations and numerical frequency calculations were performed using the TPSS functional[31] and the def2-TZVP basis set[32] for Mn, O, and N atoms and the def2-SVP basis set[33] for C and H atoms. TD-DFT calculations were performed with the B3LYP functional[34] with the def2-TZVP basis set for Mn, O, and N atoms and def2-SVP for C and H. The Hellweg RI-MP2 (C) auxiliary basis set def2-TZVP/C[35] was also used for the TD-DFT calculations. Single-point energy calculations employed the hybrid TPSSh functional with the large def2-TZVPP basis set for all atoms. For all calculations, solvation effects were included using the CPCM SMD solvation model for DMF as implemented in ORCA.[36] Additional information related to the electronic structure calculations is included in the SI.

Acknowledgements

N.K. acknowledges funding from the French government for his Ph.D.; T.A.J. acknowledges funding from the U.S. National Science Foundation. This project began with an international supplement to NSF CHE-1056470, which supported A.A.M.'s work. The project was completed with support from NSF CHE-1900384. The Mn^{II} complex used for this study was synthesized by Dr. Derek Rice.

Keywords: O–O activation • peroxido ligands • cyclic voltammetry • UV/Vis spectroelectrochemistry • DFT calculation

[1] M. E. Stroupe, M. DiDonato, J. A. Tainer, in *Encyclopedia of Inorganic and Bioinorganic Chemistry*, **2011**.
[2] J. W. Whittaker, *Arch. Biochem. Biophys.* **2012**, *525*, 111-120.
[3] A. Wennman, E. H. Oliw, S. Karkehabadi, Y. Chen, *J. Biol. Chem.* **2016**, *291*, 8130-8139.
[4] J. Yano, J. Kern, K. Sauer, M. J. Latimer, Y. Pushkar, J. Biesiadka, B. Loll, W. Saenger, J. Messinger, A. Zouni, V. K. Yachandra, *Science* **2006**, *314*, 821-825.
[5] J. Messinger, *Phys. Chem. Chem. Phys.* **2004**, *6*, 4764-4771.
[6] a) X. Huang, J. T. Groves, *Chem. Rev.* **2018**, *118*, 2491-2553; b) S. M. Adam, G. B. Wijeratne, P. J. Rogler, D. E. Diaz, D. A. Quist, J. J. Liu, K. D. Karlin, *Chem. Rev.* **2018**, *118*, 10840-11022.
[7] a) C. Policar, S. Durot, F. Lambert, M. Cesario, F. Ramiandrasoa, I. Morgenstern-Badarau, *Eur. J. Inorg. Chem.* **2001**, *2001*, 1807-1818; b) S. Durot, C. Policar, F. Cisnetti, F. Lambert, J.-P. Renault, G. Pelosi, G. Blain, H. Korri-Youssoufi, J.-P. Mahy, *Eur. J. Inorg. Chem.* **2005**, *2005*, 3513-3523; c) S. Groni, G. Blain, R. Guillot, C. Policar, E. Anxolabéhère-Mallart, *Inorg. Chem.* **2007**, *46*, 1951-1953; d) D. F. Leto, S. Chattopadhyay, V. W. Day, T. A. Jackson, *Dalton Trans.* **2013**, *42*, 13014-13025; e) H. E. Colmer, A. W. Howcroft, T. A. Jackson, *Inorg. Chem.* **2016**, *55*, 2055-2069.
[8] a) N. Kitajima, H. Komatsuzaki, S. Hikichi, M. Osawa, Y. Moro-oka, *J. Am. Chem. Soc.* **1994**, *116*, 11596-11597; b) U. P. Singh, A. K. Sharma, S. Hikichi, H. Komatsuzaki, Y. Moro-oka, M. Akita, *Inorg. Chim. Acta* **2006**, *359*, 4407-4411; c) S. Groni, P. Dorlet, G. Blain, S. Bourcier, R. Guillot, E. Anxolabéhère-Mallart, *Inorg. Chem.* **2008**, *47*, 3166-3172; d) R. A. Geiger, S. Chattopadhyay, V. W. Day, T. A. Jackson, *J. Am. Chem. Soc.* **2010**, *132*, 2821-2831; e) R. A. Geiger, S. Chattopadhyay, V. W. Day, T. A. Jackson, *Dalton Trans.* **2011**, *40*, 1707-1715; f) R. A. Geiger, D. F. Leto, S. Chattopadhyay, P. Dorlet, E. Anxolabéhère-Mallart, T. A. Jackson, *Inorg. Chem.* **2011**, *50*, 10190-10203; g) R. A. Geiger, G. B. Wijeratne, V. W. Day, T. A. Jackson, *Eur. J. Inorg. Chem.* **2012**, *2012*, 1598-1608; h) M. S. Seo, J. Y. Kim, J. Annaraj, Y. Kim, Y.-M. Lee, S.-J. Kim, J. Kim, W. Nam, *Angew. Chem. Int. Ed.* **2007**, *46*, 377-380; i) J. Annaraj, J. Cho, Y.-M. Lee, S. Y. Kim, R. Latifi, S. P. de Visser, W. Nam, *Angew. Chem. Int. Ed.* **2009**, *48*, 4150-4153; j) M. C. Denler, G. B. Wijeratne, D. B. Rice, H. E. Colmer, V. W. Day, T. A. Jackson, *Dalton Trans.* **2018**, *47*, 13442-13458; k) J. Du, D. Xu, C. Zhang, C. Xia, Y. Wang, W. Sun, *Dalton Trans.* **2016**, *45*, 10131-10135; l) D. D. Narulkar, A. Ansari, A. K. Vardhaman, S. S. Harmalkar, G. Lingamallu, V. M. Dhavale, M. Sankaralingam, S. Das, P. Kumar, S. N. Dhuri, *Dalton Trans.* **2021**, *50*, 2824-2831.
[9] a) R. L. Shook, W. A. Gunderson, J. Greaves, J. W. Ziller, M. P. Hendrich, A. S. Borovik, *J. Am. Chem. Soc.* **2008**, *130*, 8888-8889; b) R. L. Shook, S. M. Peterson, J. Greaves, C. Moore, A. L. Rheingold, A. S. Borovik, *J. Am. Chem. Soc.* **2011**, *133*, 5810-5817.
[10] a) S. Durot, F. Lambert, J.-P. Renault, C. Policar, *Eur. J. Inorg. Chem.* **2005**, *2005*, 2789-2793; b) Y. Nishida, N. Tanaka, A. Yamazaki, T. Tokii, N. Hashimoto, K. Ide, K. Iwasawa, *Inorg. Chem.* **1995**, *34*, 3616-3620; c) D. E. Cabelli, B. H. J. Bielski, *The Journal of Physical Chemistry* **1984**, *88*, 3111-3115; d) K. Barnese, E. B. Gralla, D. E. Cabelli, J. Selverstone Valentine, *J. Am. Chem. Soc.* **2008**, *130*, 4604-4606.
[11] a) J. S. Valentine, A. E. Quinn, *Inorg. Chem.* **1976**, *15*, 1997-1999; b) J. N. Burstyn, J. A. Roe, A. R. Miksztal, B. A. Shaevitz, G. Lang, J. S. Valentine, *J. Am. Chem. Soc.* **1988**, *110*, 1382-1388; c) C. J. Weschler, B. M. Hoffman, F. Basolo, *J. Am. Chem. Soc.* **1975**, *97*, 5278-5280; d) B. M. Hoffman, C. J. Weschler, F. Basolo, *J. Am. Chem. Soc.* **1976**, *98*, 5473-5482; e) B. M. Hoffman, T. Szymanski, T. G. Brown, F. Basolo, *J. Am. Chem. Soc.* **1978**, *100*, 7253-7259; f) R. B. VanAtta, C. E. Strouse, L. K. Hanson, J. S. Valentine, *J. Am. Chem. Soc.* **1987**, *109*, 1425-1434.
[12] S. El Ghachtouli, H. Y. Ching, B. Lassalle-Kaiser, R. Guillot, D. F. Leto, S. Chattopadhyay, T. A. Jackson, P. Dorlet, E. Anxolabéhère-Mallart, *Chem Commun (Camb)* **2013**, *49*, 5696-5698.
[13] N. Ségaud, E. Anxolabéhère-Mallart, K. Sénéchal-David, L. Acosta-Rueda, M. Robert, F. Banse, *Chem. Sci.* **2015**, *6*, 639-647.
[14] R. Oliveira, W. Zouari, C. Herrero, F. Banse, B. Schöllhorn, C. Fave, E. Anxolabéhère-Mallart, *Inorg. Chem.* **2016**, *55*, 12204-12210.
[15] N. Kostopoulos, F. Banse, C. Fave, E. Anxolabehere-Mallart, *Chem Commun (Camb)* **2021**, *57*, 1198-1201.
[16] H. Y. V. Ching, E. Anxolabéhère-Mallart, H. E. Colmer, C. Costentin, P. Dorlet, T. A. Jackson, C. Policar, M. Robert, *Chem. Sci.* **2014**, *5*, 2304.
[17] a) J. D. Parham, G. B. Wijeratne, D. B. Rice, T. A. Jackson, *Inorg. Chem.* **2018**, *57*, 2489-2502; b) D. B. Rice, S. D. Jones, J. T. Douglas, T. A. Jackson, *Inorg. Chem.* **2018**, *57*, 7825-7837; c) D. B. Rice, E. N. Grotemeyer, A. M. Donovan, T. A. Jackson, *Inorg. Chem.* **2020**, *59*, 2689-2700; d) G. B. Wijeratne, V. W. Day, T. A. Jackson, *Dalton Trans.* **2015**, *44*, 3295-3306; e) D. B. Rice, G. B. Wijeratne, A. D. Burr, J. D.

Parham, V. W. Day, T. A. Jackson, *Inorg. Chem.* **2016**, *55*, 8110-8120.
[18] J. D. Parham, G. B. Wijeratne, J. R. Mayfield, T. A. Jackson, *Dalton Trans.* **2019**, *48*, 13034-13045.
[19] a) C. Hureau, E. Anxolabéhère-Mallart, M. Nierlich, F. Gonnet, E. Rivière, G. Blondin, *Eur. J. Inorg. Chem.* **2002**, *2002*, 2710-2719; b) S. Groni, C. Hureau, R. Guillot, G. Blondin, G. Blain, E. Anxolabéhère-Mallart, *Inorg. Chem.* **2008**, *47*, 11783-11797.
[20] J.-M. Saveant, in *Elements of Molecular and Biomolecular Electrochemistry*, **2006**, pp. 251-297.
[21] J.-M. Saveant, in *Elements of Molecular and Biomolecular Electrochemistry* (Ed.: J.-M. Saveant), **2006**, pp. 182-250.
[22] a) A. A. Ameen, A. N. Giordano, J. R. Alston, M. W. Forney, N. P. Herring, S. Kobayashi, S. G. Ridlen, S. S. Subaran, T. J. Younts, J. C. Poler, *Phys. Chem. Chem. Phys.* **2014**, *16*, 5855-5865; b) A. C. Brezny, S. I. Johnson, S. Raugei, J. M. Mayer, *J. Am. Chem. Soc.* **2020**, *142*, 4108-4113.
[23] W. A. Gunderson, A. I. Zatsman, J. P. Emerson, E. R. Farquhar, L. Que, J. D. Lipscomb, M. P. Hendrich, *J. Am. Chem. Soc.* **2008**, *130*, 14465-14467.
[24] H. Komatsuzaki, N. Sakamoto, M. Satoh, S. Hikichi, M. Akita, Y. Moro-oka, *Inorg. Chem.* **1998**, *37*, 6554-6555.
[25] *We note that in simulation and DFT-calculations potentials refer to formal potentials, however electrochemical experiments can only give access to peak potentials corresponding to irreversible reduction of oxidation processes at the electrode surface.*
[26] S. N. Chowdhury, S. Biswas, P. Das, S. Paul, A. N. Biswas, *Inorg Chem* **2020**, *59*, 14012-14022.
[27] S. Biswas, S. Bose, J. Debgupta, P. Das, A. N. Biswas, *Dalton Trans* **2020**, *49*, 7155-7165.
[28] H. Y. V. Ching, E. Anxolabéhère-Mallart, H. E. Colmer, C. Costentin, P. Dorlet, T. A. Jackson, C. Policar, M. Robert, *Chemical Science* **2014**, *5*.
[29] a) Y. Hitomi, K. Arakawa, T. Funabiki, M. Kodera, *Angewandte Chemie International Edition* **2012**, *51*, 3448-3452; b) G. B. Wijeratne, B. Corzine, V. W. Day, T. A. Jackson, *Inorganic Chemistry* **2014**, *53*, 7622-7634.
[30] F. Neese, *WIREs Computational Molecular Science* **2011**, *2*, 73-78.
[31] M. Buhl, H. Kabrede, *J Chem Theory Comput* **2006**, *2*, 1282-1290.
[32] F. Weigend, R. Ahlrichs, *Phys Chem Chem Phys* **2005**, *7*, 3297-3305.
[33] F. Weigend, *Phys Chem Chem Phys* **2006**, *8*, 1057-1065.
[34] C. Lee, W. Yang, R. G. Parr, *Phys Rev B* **1988**, *37*, 785-789.
[35] A. Hellweg, C. Hättig, S. Höfener, W. Klopper, *Theoretical Chemistry Accounts* **2007**, *117*, 587-597.
[36] A. V. Marenich, C. J. Cramer, D. G. Truhlar, *J Phys Chem B* **2009**, *113*, 6378-6396.

Entry for the Table of Contents

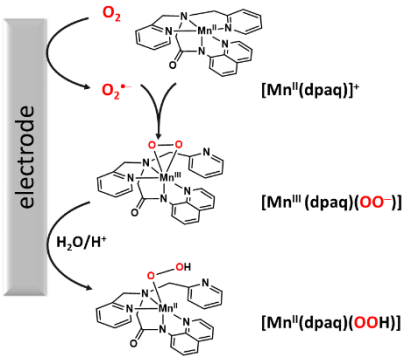

The electrochemical formation of the Mn^{III}(dpaq)(OO) complex supported on a pentadentate ligand featuring an amide moiety, and its reactivity in DMF is probed by low temperature electronic absorption spectro-electrochemistry experiments and structurally characterized using DFT computations. An analysis combining CV and simulations, corroborated by DFT computation supports the formation of a Mn^{II}(dpaq)(OOH) complex upon its reduction.